

Modelling of lattice matched dilute nitride 4-junction concentrator solar cells on Ge substrates **FREE**

Mario Ochoa; Iván García; Iván Lombardero; Luna Ayllón; Ignacio Rey-Stolle; Carlos Algora; Andrew Johnson; J. Iwan Davies; Kian Hua Tan; Wan Khai Loke; Satrio Wicaksono; Soon Fatt Yoon; Efraín Ochoa-Martínez; Mercedes Gabás



AIP Conference Proceedings 1766, 080003 (2016)

<https://doi.org/10.1063/1.4962101>



CrossMark

Articles You May Be Interested In

GaNAsSb material for ultrafast microwave photoconductive switching application

Appl. Phys. Lett. (August 2008)

Low temperature grown GaNAsSb: A promising material for photoconductive switch application

Appl. Phys. Lett. (September 2013)

GaNAsSb/GaAs waveguide photodetector with response up to 1.6 μ m grown by molecular beam epitaxy

Appl. Phys. Lett. (August 2008)

Downloaded from http://pubs.aip.org/aip/acp/article-pdf/doi/10.1063/1.4962101/13097252/080003_1_online.pdf

AIP Advances

Why Publish With Us?

- 25 DAYS**
average time to 1st decision
- 740+ DOWNLOADS**
average per article
- INCLUSIVE**
scope

[Learn More](#)

Modelling of Lattice Matched Dilute Nitride 4-junction Concentrator Solar Cells on Ge Substrates

Mario Ochoa^{1, a)}, Iván García¹, Iván Lombardero¹, Luna Ayllón¹, Ignacio Rey-Stolle¹, Carlos Algora¹, Andrew Johnson², J. Iwan Davies², Kian Hua Tan³, Wan Khai Loke³, Satrio Wicaksono³ and Soon Fatt Yoon³, Efraín Ochoa-Martínez⁴ and Mercedes Gabás⁴

¹*Instituto de Energía Solar, Universidad Politécnica de Madrid, Avda. Complutense 30, 28040 Madrid, Spain*

²*IQE plc, Cardiff, UK*

³*School of Electrical and Electronic Engineering, Nanyang Technological University, Nanyang Avenue, Singapore 639798, Republic of Singapore*

⁴*Nanotechnology Unit, Universidad de Málaga, Málaga, Spain*

^{a)}Corresponding author: mario.ochoa@ies-def.upm.es

Abstract. Technology Computer Aided Design modeling is used to examine the performance under light concentration of a 4-J solar cell Ge-based that includes a 1-eV MBE-grown dilute nitride subcell. The 1-eV solar cell is modeled and examined by using material parameters extracted from detailed electro-optical characterization prior to be included into a multijunction structure. The modelling reveals the impact of the electric field-assisted collection in the performance of single junction solar cells and its effect when included in a 4-Junction solar cells. This effect is responsible for the lower FF (~15% lower) in the 4J when including the dilute nitride subcell, especially if it limits the photocurrent. Finally, an optimization procedure based on dilute nitrides with higher material quality is performed resulting in a 4-Junction solar cell with an efficiency of 47% for concentrations between 1000-2000 suns direct terrestrial spectrum.

INTRODUCTION

Lattice-matched (LM) triple junction solar cells that incorporate dilute nitrides have reached efficiencies of 43.5% at 418 suns by using a GaInP/GaAs/GaInNAs triple junction structure grown on inactive GaAs substrates [1]. This efficiency can be exceeded using a 4-Junction device including a dilute nitride 1eV subcell which can be grown on an active germanium substrate. One of the potential limitations of the current 3-Junction dilute nitride cells is that they are grown by Molecular Beam Epitaxy (MBE) which has a moderate throughput thus being a limitation for a wide deployment required in terrestrial applications. Metal Organic Vapour Phase Epitaxy (MOVPE) has a high throughput but the poor dilute nitride material properties achieved by this technology in the past have precluded its use [2]. In order to unblock this situation we are investigating the combination of both MBE and MOVPE as a first step towards a full MOVPE process to manufacture a 4-Junction solar cell. In order to take advantage of the inclusion of a 1-eV dilute nitride solar cell into a 4-Junction structure, the following requirements must be met: 1) A J_{SC} of ~13 – 14 mA/cm² needs to be achieved for current-matching demanding high collection properties in the 1-eV subcell and 2) an efficient broadband anti-reflection coating (ARC) has to be developed. On one hand, to comply with the current-matching criteria, MBE-grown dilute nitrides have shown better photovoltaic properties than their MOVPE counterparts as demonstrated in [1]. However, the quality of the material is very dependent on specific conditions of in-situ and/or ex-situ thermal annealing treatments and their effect on the evolution of nitrogen related defects and background carrier concentration [3, 7]. Therefore, the achievement of a high quality material is not straightforward. On the other hand, incorporation of the dilute nitride subcell into the 4-junction stack leads to reduction of the light that germanium subcell can absorb. In fact, it compromises the current-matching requirement

due to lower carrier collection of germanium at long wavelengths ($\lambda > 1550\text{nm}$) and the higher reflectivity at the infrared region due to the lack of a broadband ARC. However, recent developments of broadband antireflection coatings have shown superior performance than conventional designs [8], and could be applied to this design of 4J solar cell. Accordingly, in this paper, we investigate on the realistic potential of a concentrator 4-Junction solar cell using a $\sim 1\text{-eV}$ dilute nitride subcell grown on germanium active substrates.

DILUTE NITRIDE SUBCELL MODELLING AND EXPERIMENT

The modelling was carried out within the framework of the physically-based TCAD simulator Atlas from Silvaco® [9]. The 2-D numerical modelling is based on drift-diffusion equations and incorporates models for heterojunctions (thermionic and thermionic field emission) and tunnel junctions [9, 10]. The photo carrier generation is calculated using Generalized-Transfer Matrix Method, which is also used to evaluate antireflection coatings [9]. Radiative and non-radiative recombination mechanisms such as Shockley-Read-Hall (S-R-H) and Auger have been also considered. The front metal grid for the concentrator cell is optimized for a solar cell resulting in a shadowing factor of 3% while a front specific contact resistance of $10^{-6} \Omega \cdot \text{cm}^2$ and a metal sheet resistance of $0.1 \Omega/\text{square}$ were used. All these values have been experimentally obtained in our standard GaInP/Ga(In)As/Ge 3J solar cells.

In order to develop a realistic model for the full 4-J dilute nitride solar cell, we begin validating our models by fitting the results to the typical experimental characterization curves (EQE, dark and light I-V at various concentrations, among others) of conventional LM GaInP/Ga(In)As/Ge 3J solar cells with a multi-sun efficiency of 40%. Then, we incorporate the 1-eV dilute nitride subcell using measured material parameters such as minority carrier lifetimes, mobilities, refractive indexes, among others that serve as input data to the model. We have explored the potential of the quaternary alloy GaNAsSb MBE-grown with 2.5% nitrogen and 6.5% Sb (nominal values) as a first candidate. The 4-Junction solar cell has the following bandgaps: 1.90, 1.41, 1.04, 0.67 eV.

Determination of GaNAsSb Material Parameters

Dilute nitrides are novel materials and thus scientific literature about their photovoltaic properties is not extensive [11, 12]. Moreover, the properties of these materials are very dependent on the growth conditions and post-growth thermal treatments [4-7]. Therefore, in order to obtain actual properties of the GaNAsSb alloy suitable for modeling purposes, several characterization techniques have been applied on GaNAsSb samples with doping levels in the range of $1 \cdot 10^{17}$ and $1 \cdot 10^{18} \text{ cm}^{-3}$ for both n-type and p-type. The characterization includes variable-angle ellipsometry (VASE), Hall measurements, Time-Resolved-Photoluminescence (TRPL), among others. The majority carrier mobility has been found to be on the order of $70 \text{ cm}^2/\text{V}\cdot\text{s}$ for p-type samples with a weak sensitivity to doping density ($8 \text{ cm}^2/\text{V}\cdot\text{s}$ difference between $1 \cdot 10^{17}$ and $1 \cdot 10^{18} \text{ cm}^{-3}$ doping level) while n-type samples showed a mobility of 266 and $128 \text{ cm}^2/\text{V}\cdot\text{s}$ for $1 \cdot 10^{17}$ and $5 \cdot 10^{17}$, respectively. By using TRPL, we have determined the surface recombination velocity between GaAs/GaNAsSb to be on the order of 10^3 cm/s and lifetimes within the range of 0.1-0.5 ns for both p-type and n-type samples in agreement with reference [3]. By using the experimental optical constants (n , k) calculated from ellipsometry measurements, the thickness requirement is estimated to be higher than $2 \mu\text{m}$ in order to ensure a high light collection ($>95\%$) while an absorber of $3 \mu\text{m}$ would collect about 98% of the incoming light for the ASTM-G1703 direct terrestrial reference spectrum.

Model Validation and Electrical Performance of the GaNAsSb Solar Cell

The electrical performance of GaNAsSb MBE-grown solar cells with the structure shown in Table 1 has been evaluated experimentally and theoretically. The external quantum efficiency (EQE) and reflectivity measurements are shown in Fig. 1.a along with the corresponding simulation data fitting.

TABLE 1. Semiconductor layer structure of GaNAsSb solar cells with nominal thicknesses and doping levels. The required thickness values to achieve the data fitting of Fig. 1 are highlighted in red.

Layer	Thickness (nm)	Doping level (cm ⁻³)
GaAs – contact	50	n ⁺ , 5·10 ¹⁸
Al _{0.7} Ga _{0.3} As – window	50/28	n, 5·10 ¹⁷
GaAs – emitter 1	100/110	n, 5·10 ¹⁷
GaNAsSb – emitter 2	100	n, 1·10 ¹⁷
GaNAsSb – base	1000	p, 5·10 ¹⁵ (u-i-d)
GaAs – buffer	300	p ⁺ , 1·10 ¹⁸
GaAs – substrate	350,000	p ⁺ , 5·10 ¹⁸

As can be seen in Fig 1.a, at mid-wavelengths (between 700-870 nm), there is an important disagreement of about 5-6% deviation between experimental and simulated EQE as can be seen in the bottom of Fig. 1.a. The excellent agreement between measured and calculated reflectivity indicates that the large deviation in mid-wavelengths was not attributed to the amount of light reflected by the solar cell. Possible causes of this discrepancy may be related to non-uniformities in the doping profile at the p-n junction or to the role of nitrogen-defects related charge accumulation, which does not follow the classical S-R-H statistics used. Nevertheless, the very good agreement (only 1% of J_{SC} deviation) in the wavelength range of interest for this 1 eV subcell inside a 4-Junction solar cell (885-1200 nm) enables the use of the model.

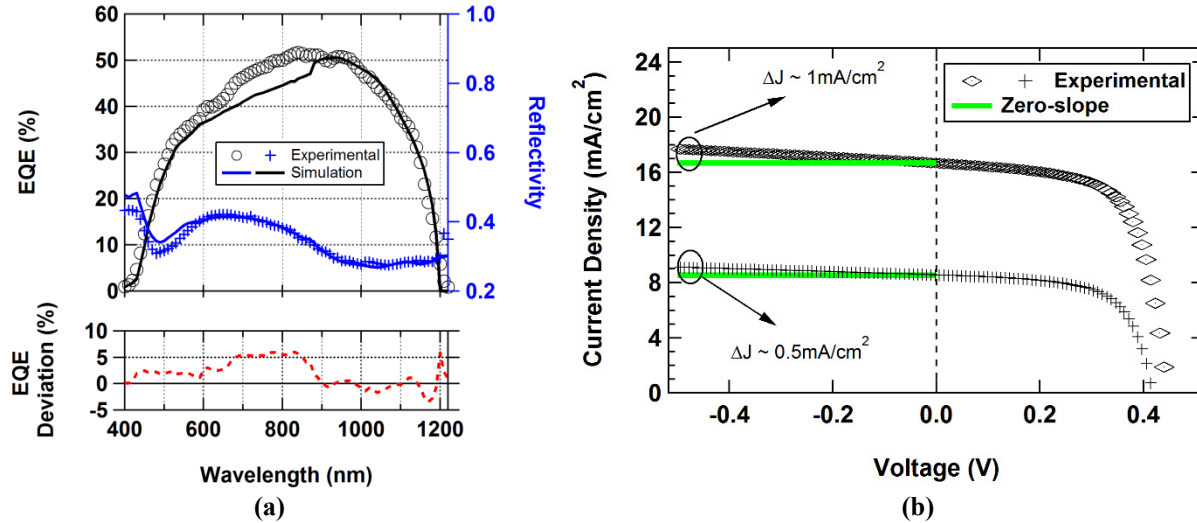


FIGURE 1. (a) Top graph depicts experimental and simulated EQE and reflectivity of GaNAsSb solar cells grown by MBE with the structure shown in Table 1. Bottom graph shows the absolute percentage deviation between experimental and simulated EQEs. (b) Experimental light I-V curves using a 940-nm LED –which is only absorbed in the GaNAsSb region– with intensities close to 1 sun (circles) and 2 suns (diamonds). No ARC has been applied onto the solar cells. These solar cells have a FF=66%, a bandgap-offset voltage $E_g/q-V_{OC} \sim 600\text{mV}$ and produces the 60% of J_{SC} required in a 4-Junction device.

The extracted minority diffusion length from the EQE fitting is 82 nm for holes at the emitter ($\mu_p = 20 \text{ cm}^2/\text{V}\cdot\text{s}$, $\tau_p = 0.14 \text{ ns}$) and 140 nm for electrons at the base ($\mu_n = 33 \text{ cm}^2/\text{V}\cdot\text{s}$, $\tau_n = 0.2 \text{ ns}$). Due to this low carrier collection property, most of the collected current comes from the space charge region, which indicates a high dependence on the electric field. In fact, experimental I-V curves (Fig. 1.b) show a non-zero slope at small reverse bias –a sort of shunt-like behavior–, which confirms the electric-field aided collection and in agreement with I-V curves and EQE data in [7].

Since the performance of the GaNAsSb solar cells is strongly dependent on the electric field distribution at the p-n junction, simulations with different base doping levels and thicknesses have been performed to evaluate the impact of the p-n junction configuration. Fig. 2.a depicts a contour plot of the EQE values at 1000 nm for different base thicknesses (W_b) and doping levels (N_A). Since most of the collection is electric-field assisted, the diffusion lengths of carriers are fixed to the values extracted from Fig. 1.a in order to evaluate the impact of different electric field

profiles as a function of doping and thickness. As can be seen, for $W_b > 700$ nm and $N_A > 2 \cdot 10^{15}$ cm⁻³, higher doping level reduces the EQE mainly due to the smaller depletion width at the base region (X_p , for electric field about 1% of the peak value found at the junction) as can be seen in Fig. 2.b. For $N_A < 2 \cdot 10^{15}$ cm⁻³, the trend is broken and the EQE values decrease with lowering doping levels. By lowering N_A from $5 \cdot 10^{15}$ cm⁻³ to $5 \cdot 10^{14}$ cm⁻³ for 2 μ m base thickness, the EQE drops from 49% to 43%. This indicates that carrier collection is not only a function of the depletion width but it is also dependent on the field intensity, as can be seen in Fig. 2.b where the black line ($N_A = 5 \cdot 10^{14}$ cm⁻³) has a higher X_p but shows the lowest electric field peak (18000 V/cm). This establishes a minimum electric field threshold required to drift carriers across the junction. For N_A similar or higher to N_D (GaNaNsSb emitter doping = 10^{17} cm⁻³), the collection is very low (32-37%) and insensitive to the thickness. The EQE is also insensitive to thickness for $W_b > 700$ nm and $N_A > 2 \cdot 10^{15}$ cm⁻³ and lower than N_D (10^{17} cm⁻³) which indicates that for the diffusion lengths achieved higher thicknesses would not enhance the collection (700 nm absorber thickness is able to get very similar carrier collection than any other higher thickness). For $W_b < 700$ nm and $N_A < 10^{16}$ cm⁻³, the low light absorption reduces substantially the EQE ($\sim 10\%$). Accordingly, the current-matching requirement could not be met through changes in doping or thickness to the present structure. In order to increase the photocurrent, some of the possibilities are: 1) enhancement of the diffusion length of carriers or 2) design of ad-hoc structures that potentially favor higher depletion widths complying with minimal critical magnitudes of electric field at the absorber.

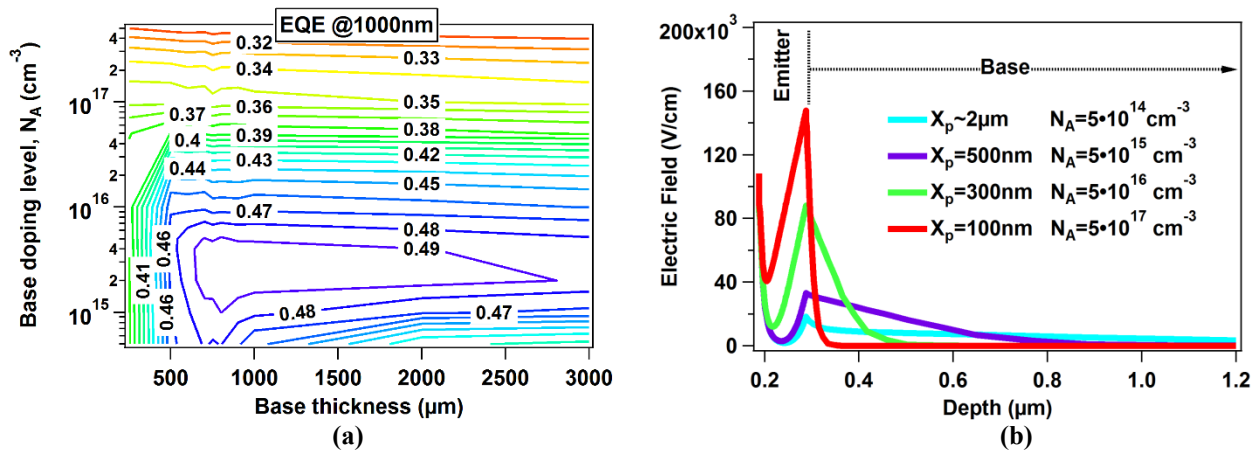


FIGURE 2. (a) Contour plot of the EQE values under 1000 nm monochromatic light for different N_A and W_b . (b) Electric field profile across the p-n junction for different N_A values for solar cells with $W_b = 2 \mu$ m. The profile has been limited to a depth of 1.2 μ m for clarity.

MODELING THE PERFORMANCE OF 4-JUNCTION SOLAR CELLS

Dilute nitride solar cells that have low photocurrents and electric field-assisted carrier collection can be detrimental to the overall performance of a 4-Junction device. This is not only in terms of current matching, but also for the FF. This can be seen in Fig. 3 where the simulated I-V curve of the 4-J device is shown together with the corresponding I-V curves of each subcell. At V_{OC} , all subcells are working in forward bias. At a limiting photocurrent of ~ 4.7 A/cm² and close to the maximum power point (MPP) of the dilute nitride subcell (0.55 V), the shunt-like behaviour of the dilute nitride subcell starts to dominate the 4J device performance resulting in a poor FF (73%). We have estimated that the FF could recover up to 87% if the solar cell were top cell limited (i.e if neither GaNaNsSb nor the Ge subcell limited the performance). However, this would require some light transfer from the other subcells which is not desirable. Interestingly, the J_{SC} of the 4J does not correspond to the lowest J_{SC} among subcells (that of dilute nitride ~ 5.7 A/cm²) but it is indeed higher around 6.3 A/cm². This is because at short-circuit of the 4J solar cell, the dilute nitride subcell is operating under reverse bias (see red points of Fig. 3) at -2.5V, being this voltage the sum of the other subcells V_{OC} 's. This is attributed to the non-zero slope photocurrent of the dilute nitride subcell both at near short circuit conditions and in reverse bias (between -2.5V and 0V) as a result of the electric-field assisted collection which is dependent on voltage. Similar trends have been already reported for a GaInAsP/InGaAs dual-junction solar cell [13]. Therefore, it can be concluded that the electric field-assisted increase of the carrier collection and J_{sc} is not useful to increase the efficiency of this subcell. Beyond the obvious but so far

elusive way to increase the carrier collection is to improve the carrier diffusion length (i.e., the material quality). Other approaches could be directed towards reducing the length the carriers have to travel to the junction, for example by using Bragg reflectors to reduce the absorber layer thickness needed.

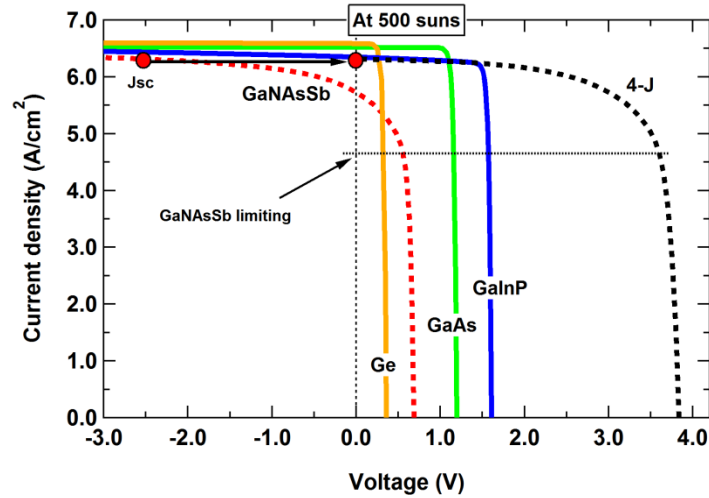


FIGURE 3. Simulated subcells and 4-Junction I-V curves under 500-suns ASTM G173 direct reference spectrum.

Although GaNAsSb nitride alloy has not fulfilled the J_{SC} requirement to be useful in a 4J solar cell, GaInNASb has already demonstrated superior performance [1]. Accordingly, in the following, we will use dilute nitride material diffusion lengths for the material (i.e. any Ga(In)NAs(Sb) material) similar to those already achieved experimentally [1, 4-6] (in the order of 10 times higher than the ones extracted from the EQE in Fig. 1.a), in order to explore the potential of the 4J solar cell. A 4J device made up of GaInP[1.9]/GaAs[1.4]/Ga(In)NAs(Sb)[1.04]/Ge[0.67] subcells is simulated. In order to usefully incorporate the Ga(In)NAs(Sb) into a 4Junction device, the demands on this material in terms of photocurrent are very high because this subcell receives the lowest spectral power density (the maximum photocurrent under ideal collection efficiency is 14.2 mA/cm^2 while for the other subcells it is about 16 mA/cm^2). For the AM1.5d G173 spectrum the Ga(In)NAs(Sb) subcell would require a higher amount of light, so the subcell on top of it must be thinned. Another possibility would be to lower the bandgap of the dilute nitride. However, care must be taken because this could make the 4th subcell (Ge) limit the photocurrent depending on its spectral response and the ARC design. By tuning the thicknesses, the device performance limitation by 3rd or 4th subcell can be avoided. The resulting concentrator structure has an absorber thickness of 1.1, 0.8, 0.525 μm for GaInP, GaAs and Ga(In)NAs(Sb), respectively.

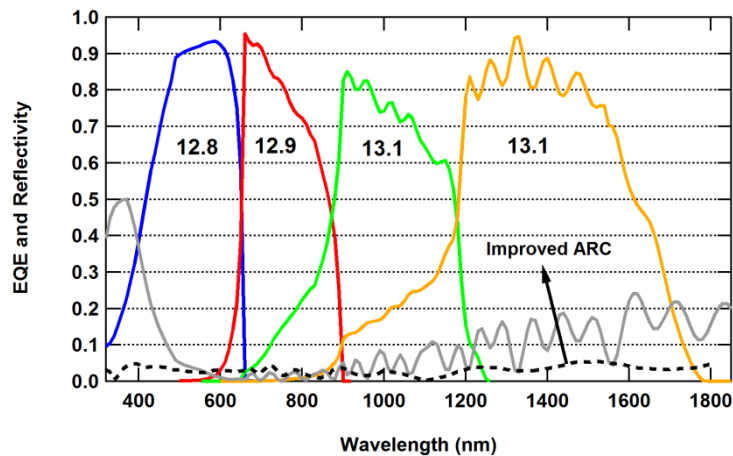


FIGURE 4. (a) Simulated External Quantum Efficiency and reflectivity of GaInP/GaAs/ Ga(In)NAs(Sb)/Ge (from left to right) 4-J solar cell analyzed in this work. The structure assumes a conventional $\text{MgF}_2(110\text{nm})/\text{ZnS}(60\text{nm})$ ARC (gray line). The improved ARC taken from [8] is represented by a black dashed line.

As can be seen in Fig. 5, for a device representative of Fig. 4 whose ARC does not provide low reflectivity in the whole spectrum range the peak efficiency is ~44% within the 1000 - 2000 suns range (red dashed line). In this respect, further improvement can be achieved by taking into account the low reflectivity offered by a broadband ARC (<5% in the whole spectrum range) as already demonstrated in [8]. By including this improved ARC and tweaking absorber thicknesses to redistribute the subsequent gains in photocurrent, the projected peak efficiency would be ~47% at 1000 suns (green line), with the increase mostly resulting from the increment in J_{SC} (12.8→13.7 mA/cm²) and to a lower extent in V_{OC} (~8 mV at 1000 suns). Above 2000 suns, series resistance due to the metal grid starts to limit the performance. The values shown in Fig. 5 correspond to the present material quality of these devices intending to provide realistic efficiencies that can be achieved in the short-term.

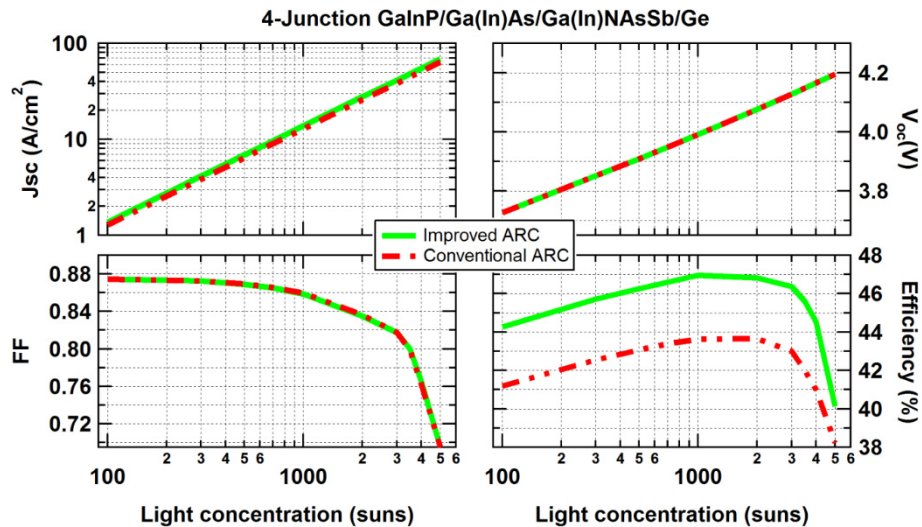


FIGURE 5. J_{SC} , V_{OC} , FF and Efficiency of a 4-Junction solar cell. Red lines represent a device whose EQE performance is shown in Fig. 4 with a J_{SC} of 12.8 mA/cm² at 1-sun while green lines correspond to a cell with an improved broadband ARC resulting in a J_{SC} =13.7 mA/cm². The difference in efficiency for both curves (improved and conventional bilayer) is mainly due to the J_{SC} difference (about 7% which is barely appreciated in top figure due to log scale plot).

Currently, we are in the stage of optimizing the 3rd and 4th subcells which are grown by MBE and MOVPE, respectively. We have also grown a complete 4-Junction solar cell (GaInP/GaAs/GaNAsSb/Ge) in order to explore the impact of the combination of MOVPE+MBE growth technologies. The performance of this 4-Junction solar cell will be analyzed shortly.

SUMMARY AND CONCLUSIONS

The potential of 4-junction lattice-matched dilute nitride solar cells for CPV applications has been studied. A realistic modeling has been developed based upon an extensive dilute nitride material characterization. The modeling shows that the shunt-like behavior, caused by the electric field-assisted carrier collection, and the low FF of the dilute nitride subcell substantially degrade the performance of a 4-Junction solar cell. This limits the potential of using the electric field-assisted carrier collection and indicates that the clearer (but so far elusive) path to achieve very high efficiencies is to improve the diffusion lengths of minority carriers by improving the quality of the dilute nitride cell. By using similar minority carrier properties for dilute nitride solar cells as the best found in the literature and using an optimized broadband ARC, the optimization of a GaInP[1.9]/GaAs[1.4]/Ga(In)NAs(Sb)[1.04]/Ge[0.67] concentrator 4J cell results in efficiencies above 47%. In order to realize this empirically, further improvement of the present dilute nitride material quality is required. Future works include the corresponding annealing treatments to further increase the material quality of the GaNAsSb, the realization of the broadband ARC and the fabrication of the whole 4-Junction already grown by combining MBE+MOVPE technologies.

ACKNOWLEDGMENTS

This work has been supported by the Spanish MINECO through the projects TEC2014-54260-C3-3-P and TEC2014-54260-C3-1-P, PCIN-2015-181-C02-01, PCIN-2015-181-C02-02 and by the Comunidad de Madrid through the project MADRID-PV (S2013/MAE-2780). European Commission has also contributed by means of the LONGESST project ([FP7](#) grant Agreement Number 607153). IQE has subcontracted NTU within the frame of the LONGESST project.

REFERENCES

1. V. Sabnis, H. Yuen, and M. Wiemer, "High-efficiency multijunction solar cells employing dilute nitrides," in [AIP Conference Proceedings](#), 2012, vol. 1477, pp. 14–19.
2. D. J. Friedman, A. J. Ptak, S. R. Kurtz, and J. F. Geisz, "Analysis of depletion-region collection in GaInNAs solar cells," *Conf. Rec. Thirty-first IEEE Photovolt. Spec. Conf. 2005.*, no. February, pp. 4–7, 2005.
3. T. Thomas, M. Fuhrer, D. A. Alvarez, N. Ekins-Daukes, K. H. Tan, S. Wicaksono, W. K. Loke, S. F. Yoon, and A. Johnson, "GaInNAsSb 1-eV solar cells for use in lattice-matched multi-junction architectures," in Conference record of the 40th IEEE Photovoltaic Specialists Conference, 2014, pp. 0550–0553.
4. K. H. Tan, S. Wicaksono, W. K. Loke, D. Li, S. F. Yoon, E. A. Fitzgerald, S. A. Ringel, and J. S. Harris Jr., "Molecular beam epitaxy grown GaInNAsSb 1eV photovoltaic cell," [J. Cryst. Growth](#), vol. 335, no. 1, pp. 66–69, Nov. 2011.
5. V. Polojärvi, A. Aho, A. Tukiainen, M. Raappana, T. Aho, A. Schramm, and M. Guina, "Influence of As/group-III flux ratio on defects formation and photovoltaic performance of GaInNAs solar cells," [Sol. Energy Mater. Sol. Cells](#), vol. 149, pp. 213–220, 2016.
6. N. Miyashita, N. Ahsan, and Y. Okada, "Generation and collection of photocarriers in dilute nitride GaInNAsSb solar cells," [Progress in Photovoltaics Research and Applications](#), vol. 24, no. 1, pp. 28–37, Jun. 2016.
7. N. Miyashita, N. Ahsan and Y. Okada, "Characterization of 1.0 eV GaInNAsSb Solar Cells for Multijunction Applications and the Effect of Annealing," in proceedings of the 31st European Photovoltaic Solar Energy Conference and Exhibition, Hamburg, 2015, n/a.
8. E. E. Perl, C. T. Lin, W. E. McMahon, D. J. Friedman, and J. E. Bowers, "Ultrabroadband and wide-angle hybrid antireflection coatings with nanostructures," [IEEE J. Photovoltaics](#), vol. 4, no. 3, pp. 962–967, 2014.
9. Silvaco software, "Atlas User's Manual", 2015
10. M. Baudrit and C. Algora, "Tunnel diode modeling, including nonlocal trap-assisted tunneling: A focus on III-V multijunction solar cell simulation," [IEEE Trans. Electron Devices](#), vol. 57, no. 10, pp. 2564–2571, 2010.
11. J.-C. Harmand, A. Caliman, E. V. K. Rao, L. Largeau, J. Ramos, R. Teissier, L. Travers, G. Ungaro, B. Theys, and I. F. L. Dias, "GaInNAsSb: how does it compare with other dilute III V-nitride alloys?," [Semicond. Sci. Technol.](#), vol. 17, no. 8, pp. 778–784, Aug. 2002.
12. D. B. Jackrel, S. R. Bank, H. B. Yuen, M. a. Wistey, J. S. Harris, A. J. Ptak, S. W. Johnston, D. J. Friedman, and S. R. Kurtz, "Dilute nitride GaInNAs and GaInNAsSb solar cells by molecular beam epitaxy," [J. Appl. Phys.](#), vol. 101, no. 11, pp. 1–8, 2007.
13. A. Braun, N. Szabó, K. Schwarzburg, T. Hannappel, E. a. Katz, and J. M. Gordon, "Current-limiting behavior in multijunction solar cells," [Appl. Phys. Lett.](#), vol. 98, no. 22, pp. 3–5, 2011.